M&C 2017 - International Conference on Mathematics & Computational Methods Applied to Nuclear Science & Engineering, Jeju, Korea, April 16-20, 2017, on USB (2017)

Nonlinear Diffusion Acceleration in Voids for the Weighted Least-Square Transport Equation

Hans R. Hammer[1], Jim E. Morel[1], and Yaqi Wang[2]

[1]*Texas A&M University - Department of Nuclear Engineering, 3133 TAMU, College Station, TX 77843-3133*
[2]*Idaho National Laboratory, 1955 N. Fremont Ave, Idaho Falls, ID 83415*

hans.hammer@tamu.edu, morel@tamu.edu, yaqi.wang@inl.gov

Abstract - *The nonlinear diffusion acceleration (NDA) is an effective scheme to increase convergence for highly diffusive problems. However, for second order transport equations, the scheme is not yet defined in voids. In this paper we derive modifications to the NDA to handle problems containing void regions. A Fourier analysis shows that the newly developed modifications accelerates unconditionally for scattering ratios smaller than one. Numerical test with Reed's problem showed that the NDA scheme results in a non-constant flux shape in the void regions. Further investigations revealed that this coarse mesh problem is caused by the interface coupling between void and material regions.*

I. INTRODUCTION

Our application encompasses detailed calculations of modern nuclear reactors. Current development in modeling and simulation raised the needs for tools which are able to handle voids or near voids. While this is definitely possible with the first order transport equation, second order schemes often show singularities and condition or convergence problems for (near) zero total cross sections. However, second order forms of the transport equation offer the advantage of using continuous finite elements (CFEM) as opposed to discontinuous finite elements (DFEM), which is especially appealing with mesh frameworks with well-developed support for CFEM, including Idaho National Laboratory's multiphysics framework MOOSE [1].

Least-squares (LS) forms of the transport equation can circumvent the void problems of other second order forms, but are non-conservative, which explains why they are not commonly used in the nuclear community. A newly developed form of least-squares transport equation is compatible with voids and standard solution techniques, but is also non-conservative [2], conservation of particles is only achieved as the numerical solution converges to the analytical solution. Introducing a weight function to this LS equation improves issues with the causality and can render our equation equal to the Self-Adjoint Angular flux (SAAF) equation [3]. The conservation issue can be ameliorated by the use of the nonlinear diffusion acceleration. While this acceleration scheme significantly decreases computational cost, it also ensures conservation if a conservative low order equation is used. In order to achieve conservation of the low order equation, it must be inconsistent with the high order LS equation. This leads to identical high order and low order solutions only in the limit as the spatial mesh is increasingly refined [4].

While the high order LS equation is valid in voids, the nonlinear diffusion acceleration employs a low order diffusion equation. This equation does not hold in void due to the definition of the classical local diffusion coefficient. We solve this by using a nonlocal formulation of the diffusion coefficient that is well defined in voids [5, 6]. Additionally, the drift vector, a correction term in the low-order equation informed by the high order equation, is also not defined in a void. We propose in this paper a combination of current formulations, which we found using a Fourier analysis and that holds in voids and is stable and efficient.

II. THEORY

1. Weighted Least-Squares Equation

The standard least-squares (LS) form of the transport equation [7] is not compatible with source iterations. The Least-Squares Equation derived by Hansen et al. [2] is a second order transport equation that is compatible with voids. In contrast to traditional least-squares equations, this equation is also usable with iterative solutions techniques e.g. source iterations with or without acceleration.

The weighted least-squares (WLS) transport equation addresses some issues of the unweighted LS equation on material interfaces and in voids. Due to the second order nature of the LS equation, downstream information can influence the upstream solution. An optically thick material further downstream in the current direction reduces the flux in the unweighted LS. Therefore the LS equation does not have causality. This is a coarse mesh problem and decreases with increasing refinement of the mesh. The introduction of a weight function diminishes this problem significantly.

Consider the transport equation in operator form

$$\mathcal{L}\psi = \mathcal{S}\psi + \mathcal{F}\psi + Q \tag{1}$$

with the linear operators

$$\mathcal{L} = \mathbf{\Omega}\cdot\mathbf{\nabla} + \sigma_{\mathrm{t}} \tag{2}$$

and $\mathcal{S}$ the scattering operator, $\mathcal{F}$ the fission operator and Q contains all remaining sources. The adjoint of the streaming and collision operator $\mathcal{L}$ under the standard inner product

$$\left(\cdot\ ,\ \cdot\right)_{\mathcal{D}} = \int_{\mathcal{D}}\int_{4\pi}\int_{0}^{\infty} dE\ d\mathbf{\Omega}\ dV \tag{3}$$

is given by

$$\mathcal{L}^{\dagger} = -\mathbf{\Omega}\cdot\mathbf{\nabla} + \sigma_{\mathrm{t}}. \tag{4}$$

Multiplying Eq. (1) with a weight function $\mathcal{W}$ and the adjoint operator Eq. (4) gives the weighted least-squares equation compatible with source iteration

$$\mathcal{L}^{\dagger}\mathcal{W}\mathcal{L}\psi = \mathcal{L}^{\dagger}\mathcal{W}\mathcal{S}\psi + \mathcal{L}^{\dagger}\mathcal{W}Q. \tag{5}$$

The mono-energetic WLS equation hence becomes

$$\begin{aligned}
&-\mathbf{\Omega}\cdot\mathbf{\nabla}\left[w\mathbf{\Omega}\cdot\mathbf{\nabla}\psi\right] - \mathbf{\Omega}\cdot\psi\mathbf{\nabla}\left[w\sigma_{\mathrm{t}}\right] + w\sigma_{\mathrm{t}}^{2}\psi \\
&= -\mathbf{\Omega}\cdot\mathbf{\nabla}\left[w\sum_{l=0}^{L}\sum_{p=-l}^{l}\frac{2l+1}{4\pi}\mathrm{Y}_{l}^{p}\sigma_{l}\phi_{l}^{p} + w\frac{\bar{\nu}\sigma_{\mathrm{f}}}{4\pi}\phi + w\frac{q}{4\pi}\right] \\
&\quad + w\sigma_{\mathrm{t}}\sum_{l=0}^{L}\sum_{p=-l}^{l}\frac{2l+1}{4\pi}\mathrm{Y}_{l}^{p}\sigma_{l}\phi_{l}^{p} + w\frac{\sigma_{\mathrm{t}}\bar{\nu}\sigma_{\mathrm{f}}}{4\pi}\phi + w\frac{q\sigma_{\mathrm{t}}}{4\pi} \qquad (6a)
\end{aligned}$$

where w denotes a weight function. The corresponding boundary condition is

$$\psi\left(\boldsymbol{x}_{b}\right) = f\left(\mathbf{\Omega}\right), \quad \mathbf{\Omega}\cdot\boldsymbol{n} < 0, \boldsymbol{x}_{b} \in \partial\mathcal{D}. \tag{6b}$$

We utilize the S_N method and derive the weak form by multiplying Eq. (6a) with a test function ψ_m^* and integrate over the spatial domain $\mathcal{D}$. Integration by parts of all terms containing a derivative gives

$$\begin{aligned}
&\left(w\mathbf{\Omega}_m\cdot\mathbf{\nabla}\psi_m + w\sigma_{\mathrm{t}}\psi_m, \mathbf{\Omega}_m\cdot\mathbf{\nabla}\psi_m^* + \sigma_{\mathrm{t}}\psi_m^*\right)_{\mathcal{D}} \\
&\quad = \left(w\sum_{l=0}^{L}\sum_{p=-l}^{l}\frac{2l+1}{4\pi}\sigma_{l}\phi_{l}^{p}\mathrm{Y}_{l}^{p}, \mathbf{\Omega}_m\cdot\mathbf{\nabla}\psi_m^* + \sigma_{\mathrm{t}}\psi_m^*\right)_{\mathcal{D}} \\
&\qquad + \left(w\frac{1}{4\pi}\nu\sigma_{\mathrm{f}}\phi + w\frac{1}{4\pi}q, \mathbf{\Omega}_m\cdot\mathbf{\nabla}\psi_m^* + \sigma_{\mathrm{t}}\psi_m^*\right)_{\mathcal{D}} \\
&\qquad + \left\langle w\mathbf{\Omega}_m\cdot\mathbf{\nabla}\psi_m + \sigma_{\mathrm{t}}\psi_m, \left(\mathbf{\Omega}_m\cdot\hat{n}\right)\psi_m^*\right\rangle_{\partial\mathcal{D}} \\
&\qquad - \left\langle w\sum_{l=0}^{L}\sum_{p=-l}^{l}\frac{2l+1}{4\pi}\sigma_{\mathrm{Y}_{l}^{p},l}\phi_{l}^{p}, \left(\mathbf{\Omega}_m\cdot\boldsymbol{n}\right)\psi_m^*\right\rangle_{\partial\mathcal{D}} \\
&\quad - \left\langle w\frac{1}{4\pi}\nu\sigma_{\mathrm{f}}\phi + w\frac{1}{4\pi}q, \left(\mathbf{\Omega}_m\cdot\boldsymbol{n}\right)\psi_m^*\right\rangle_{\partial\mathcal{D}}, \quad m = 1\ldots M \qquad (7)
\end{aligned}$$

with the inner product Eq. (3) and

$$\left\langle\cdot\,,\,\cdot\right\rangle_{\partial\mathcal{D}} = \oint_{\partial\mathcal{D}}\int_{4\pi}\int_{0}^{\infty} dE\; d\mathbf{\Omega}\; dA \tag{8}$$

the corresponding surface integral with outwards normal $\boldsymbol{n}$.

Note that if we assume the first-order multi-group S_N transport equation is exactly met on the boundary $\partial\mathcal{D}$, all of the boundary terms cancel. An additional motivation for making this assumption is that it renders our Galerkin method for the second-order least-squares equation equivalent to the least-squares finite-element method for the first-order form of the S_N equations using the same trial space.

The natural boundary condition Eq. (6b) of Eq. (6) is a Dirichlet boundary condition. However this is difficult to implement in numerical codes. We chose to use the optional weak boundary condition

$$\left\langle f_m\left(\psi_m - \psi_m^{inc}\right), \psi_m^*\right\rangle_{\partial\mathcal{D}^-}, \quad m = 1\ldots M \tag{9}$$

instead, where $\partial\mathcal{D}^-$ is the portion of the boundary for which $\mathbf{\Omega}_m\cdot\boldsymbol{n} < 0$.

Based on the SAAF boundary condition [8] we define

$$f_m = \sigma_{\mathrm{t}}\left|\mathbf{\Omega}\cdot\boldsymbol{n}\right|. \tag{10}$$

However, the SAAF boundary conditions are defined over the whole boundary, while the optional LS boundary condition is only defined on the incoming boundary. For near void problems the choice

$$f_m = \max\left(\sigma_{\mathrm{t}}, \frac{1}{h}\right)\left|\mathbf{\Omega}\cdot\boldsymbol{n}\right| \tag{11}$$

gives a more accurate and better conditioned version. Here h denotes a characteristic length constant of the boundary cell. Another boundary condition, which often shows better results, is based on a diffusion limit analysis

$$f_m = 4\frac{\left|\mathbf{\Omega}\cdot\boldsymbol{n}\right|}{h} + \sigma_{\mathrm{t}}\left(3\left|\mathbf{\Omega}\cdot\boldsymbol{n}\right|^{2} + 2\left|\mathbf{\Omega}\cdot\boldsymbol{n}\right|\right). \tag{12}$$

By adding the boundary condition Eq. (9) to Eq. (7) we obtain the WLS weak formulation: Given a trial space $W_{\mathcal{D}}$, consisting of continuous basis functions, the weak form for a specific direction and group is as follows: Find $\psi_m^* \in W_{\mathcal{D}}$ such that

$$\begin{aligned}
&\left(w\mathbf{\Omega}_m\cdot\mathbf{\nabla}\psi_m + w\sigma_{\mathrm{t}}\psi_m, \mathbf{\Omega}_m\cdot\mathbf{\nabla}\psi_m^* + \sigma_{\mathrm{t}}\psi_m^*\right)_{\mathcal{D}} \\
&\qquad + \left\langle w f_m\left(\psi_m - \psi^{\mathrm{inc}}\right), \psi_m^*\right\rangle_{\partial\mathcal{D}^-} \\
&\quad = \left(w\sum_{g'=1}^{G}\sum_{l=0}^{L}\sum_{p=-l}^{l}\frac{2l+1}{4\pi}\mathrm{Y}_{l}^{p}\sigma_{l}\phi_{l}^{p}, \mathbf{\Omega}_m\cdot\mathbf{\nabla}\psi_m^* + \sigma_{\mathrm{t}}\psi_m^*\right)_{\mathcal{D}} \\
&\quad + \left(w\frac{1}{4\pi}\nu\sigma_{\mathrm{f}}\phi + w\frac{1}{4\pi}q, \mathbf{\Omega}_m\cdot\mathbf{\nabla}\psi_m^* + \sigma_{\mathrm{t}}\psi_m^*\right)_{\mathcal{D}}, m = 1\ldots M
\end{aligned} \tag{13}$$

The following weight function improves the thick diffusion limit [9]

$$w \equiv \frac{1}{\sigma_{\mathrm{t}}} \tag{14}$$

and makes our equations equivalent to the SAAF equation [3] if we expand the first derivative terms and neglect the optional boundary condition Eq. (9). However, the weight function Eq. (14) is not defined in voids. Introducing a limit

$$w \equiv \min\left(\frac{1}{\sigma_{\mathrm{t}}}, w_{\max}\right) \tag{15}$$

where $w_{\max}$ denotes a maximum value for the weight function makes the WLS equation well defined in voids and maintains the symmetric positive-definite properties of the resulting discretized matrix, but the WLS equation is comparable to the SAAF equation only for sufficient large total cross sections σ_{t}. Hence we decided to use Eq. (13) with optional boundary conditions Eq. (9).

2. Nonlinear Diffusion Acceleration

We derive our low order diffusion equation from the first order transport equation as shown by Peterson [4]. This results in an inconsistent, but conservative form of the NDA. Integrating the mono-energetic transport equation over all angles gives us the zeroth moment equation

$$\boldsymbol{\nabla}\cdot\boldsymbol{J}+\sigma_{\mathrm{t}}\phi=\sigma_{\mathrm{s}}\phi+q. \tag{16}$$

To close Eq. (16), we consider the first moment equation

$$\sum_{m=1}^{M}\omega_m\boldsymbol{\Omega}_m\left(\boldsymbol{\Omega}_m\cdot\boldsymbol{\nabla}\psi_{m,g}\right)+\sigma_{\mathrm{t}}\boldsymbol{J}=\sigma_1\boldsymbol{J} \tag{17}$$

with gives the current

$$\boldsymbol{J}=-\frac{1}{\sigma_{\mathrm{tr}}}\sum_{m=1}^{M}\omega_m\boldsymbol{\Omega}_m\left(\boldsymbol{\Omega}_m\cdot\boldsymbol{\nabla}\psi_m\right) \tag{18}$$

with the transport cross section

$$\sigma_{\mathrm{tr}}\equiv\sigma_{\mathrm{t}}-\sigma_1. \tag{19}$$

We use Eq. (18) to construct an additive correction to Fick's law

$$\begin{aligned}\boldsymbol{J}&=-\mathrm{D}\boldsymbol{\nabla}\phi+\mathrm{D}\boldsymbol{\nabla}\phi-\frac{1}{\sigma_{\mathrm{tr}}}\sum_{m=1}^{M}\omega_m\boldsymbol{\Omega}_m\boldsymbol{\Omega}_m\cdot\boldsymbol{\nabla}\psi_m\\&=-\mathrm{D}\boldsymbol{\nabla}\phi-\hat{D}\phi\end{aligned} \tag{20}$$

with the drift vector

$$\hat{D}\equiv\frac{1}{\phi}\left(\frac{1}{\sigma_{\mathrm{tr}}}\sum_{m=1}^{M}\omega_m\boldsymbol{\Omega}_m\left(\boldsymbol{\Omega}_m\cdot\boldsymbol{\nabla}\psi_m\right)-\mathrm{D}\boldsymbol{\nabla}\phi\right) \tag{21}$$

and the diffusion coefficient is defined as

$$\mathrm{D}\equiv\frac{1}{3\sigma_{\mathrm{tr}}}. \tag{22}$$

Substituting Eq. (20) into Eq. (16) gives a drift-diffusion equation

$$-\boldsymbol{\nabla}\cdot\left[\mathrm{D}\boldsymbol{\nabla}\phi\right]-\boldsymbol{\nabla}\cdot\left[\hat{D}\phi\right]+\sigma_{\mathrm{a}}\phi=q. \tag{23}$$

Multiplying Eq. (16) by a test function ϕ^* and integrating over the domain gives the corresponding weak form

$$\left(\boldsymbol{\nabla}\cdot\boldsymbol{J},\phi^*\right)_{\mathcal{D}}+\left(\sigma_{\mathrm{a}}\phi,\phi^*\right)_{\mathcal{D}}=\left(q,\phi^*\right)_{\mathcal{D}}. \tag{24}$$

Applying integration by parts on the current term and substituting Eq. (20) gives

$$\begin{aligned}-\left(\mathrm{D}\boldsymbol{\nabla}\phi,\boldsymbol{\nabla}\phi^*\right)_{\mathcal{D}}-\left(\hat{D}\phi,\boldsymbol{\nabla}\phi^*\right)_{\mathcal{D}}+\langle\boldsymbol{n}\cdot\boldsymbol{J},\phi^*\rangle_{\partial\mathcal{D}}\\+\left(\sigma_{\mathrm{a}}\phi,\phi^*\right)_{\mathcal{D}}=\left(q,\phi^*\right)_{\mathcal{D}}.\end{aligned} \tag{25}$$

The boundary term $\langle\boldsymbol{n}\cdot\boldsymbol{J},\phi^*\rangle_{\partial\mathcal{D}}$ still needs to be evaluated. While the reflective boundary condition is natural to the diffusion equation, the vacuum condition is more challenging. Using the partial currents we can define

$$\begin{aligned}\langle\boldsymbol{n}\cdot\boldsymbol{J},\phi^*\rangle_{\partial\mathcal{D}}&=\left\langle J^{\mathrm{out}}-J^{\mathrm{in}},\phi^*\right\rangle_{\partial\mathcal{D}}\\&=\left\langle\frac{1}{4}\kappa\phi-J^{\mathrm{in}},\phi^*\right\rangle_{\partial\mathcal{D}}\end{aligned} \tag{26}$$

with the vacuum boundary coefficient as

$$\begin{aligned}\kappa&\equiv 4\frac{J^{\mathrm{out}}}{\phi}\\&=\frac{4}{\phi}\sum_{\boldsymbol{n}\cdot\boldsymbol{\Omega}_m>0}\omega_m\left|\boldsymbol{n}\cdot\boldsymbol{\Omega}_m\right|\psi_m\end{aligned} \tag{27}$$

and substitute this into the boundary term. Note that we changed the vacuum boundary coefficient from the one described in [4] to Eq. (27) to be consistent with the SAAF implementation in Rattlesnake.

For a given iteration k the NDA scheme is defined as follows:

1. Solve the WLS transport equation

$$\begin{aligned}&\left(w\boldsymbol{\Omega}_m\cdot\boldsymbol{\nabla}\psi_m^{k+\frac{1}{2}}+w\sigma_{\mathrm{t}}\psi_m^{k+\frac{1}{2}},\boldsymbol{\Omega}_m\cdot\boldsymbol{\nabla}\psi_m^*+\sigma_{\mathrm{t}}\psi_m^*\right)_{\mathcal{D}}\\&\quad+\left\langle wf_m\left(\psi_m^{k+\frac{1}{2}}-\psi^{\mathrm{inc}}\right),\psi_m^*\right\rangle_{\partial\mathcal{D}^-}\\&=\left(w\sum_{g'=1}^{G}\sum_{l=0}^{L}\sum_{p=-l}^{l}\frac{2l+1}{4\pi}\mathrm{Y}_l^p\sigma_l\phi_l^{p,k},\boldsymbol{\Omega}_m\cdot\boldsymbol{\nabla}\psi_m^*+\sigma_{\mathrm{t}}\psi_m^*\right)_{\mathcal{D}}\\&+\left(w\frac{1}{4\pi}\nu\sigma_{\mathrm{f}}\phi^k+w\frac{1}{4\pi}q,\boldsymbol{\Omega}_m\cdot\boldsymbol{\nabla}\psi_m^*+\sigma_{\mathrm{t}}\psi_m^*\right)_{\mathcal{D}},m=1\ldots M\end{aligned} \tag{28a}$$

2. Calculate the correction terms for the diffusion equation

$$\kappa^{k+\frac{1}{2}}=\frac{4}{\phi}\sum_{\boldsymbol{n}\cdot\boldsymbol{\Omega}_m>0}\omega_m\left|\boldsymbol{n}\cdot\boldsymbol{\Omega}_m\right|\psi_m^{k+\frac{1}{2}} \tag{28b}$$

$$\hat{D}^{k+\frac{1}{2}}=\frac{1}{\phi^{k+\frac{1}{2}}}\left(\frac{1}{\sigma_{\mathrm{tr}}}\sum_{m=1}^{M}\omega_m\boldsymbol{\Omega}_m\left(\boldsymbol{\Omega}_m\cdot\boldsymbol{\nabla}\psi_m^{k+\frac{1}{2}}\right)-\mathrm{D}\boldsymbol{\nabla}\phi^{k+\frac{1}{2}}\right) \tag{28c}$$

3. Solve the diffusion equation

$$\begin{aligned}&-\left(\mathrm{D}\boldsymbol{\nabla}\phi^{k+1},\boldsymbol{\nabla}\phi^*\right)_{\mathcal{D}}-\left(\hat{D}^{k+\frac{1}{2}}\phi^{k+1},\boldsymbol{\nabla}\phi^*\right)_{\mathcal{D}}\\&+\left\langle\frac{\kappa^{k+\frac{1}{2}}}{4}\phi^{k+1}-J^{\mathrm{in}},\phi^*\right\rangle_{\partial\mathcal{D}}+\left(\sigma_{\mathrm{a}}\phi^{k+1},\phi^*\right)_{\mathcal{D}}=\left(q,\phi^*\right)_{\mathcal{D}}\end{aligned} \tag{28d}$$

4. Check convergence and update the scattering source

The iteration scheme for the NDA starts with a low order solve of Eq. (28d) assuming $\hat{D}^{\frac{1}{2}} = 0$ and $\kappa^{\frac{1}{2}} = 1$. The scalar flux is transferred to the high order system and used for the scattering and fission source. The new angular flux is obtained and the drift vector and boundary coefficient calculated. These are then used for the next low order diffusion solve. This iteration continues until convergence of the low order and high order solutions.

The derivation of the multi-group equations is similar and we leave it to the reader to do so. The only thing to be consider are the cross group scattering terms in the drift vector

$$\hat{D}_g^{k+\frac{1}{2}} \equiv \frac{1}{\phi_g^{k+\frac{1}{2}}}\left(\frac{1}{\sigma_{\mathrm{tr},g}}\sum_{m=1}^{M}\omega_m\boldsymbol{\Omega}_m\left(\boldsymbol{\Omega}_m\cdot\boldsymbol{\nabla}\psi_{m,g}^{k+\frac{1}{2}}\right)\right.$$
$$\left.-\frac{1}{\sigma_{\mathrm{tr},g}}\sum_{\substack{g'=1\\ g'\neq g}}^{G}\sigma_{1,g'\to g}\boldsymbol{J}_{g'}^{k+\frac{1}{2}}-\mathrm{D}_g\boldsymbol{\nabla}\phi_g^{k+\frac{1}{2}}\right). \quad (29)$$

3. Modifications for void

The classical formulation of the diffusion coefficient (Eq. (22)) does not hold in voids. However, if we consider Eq. (20) we see that in the case of spatial and iterative convergence, the diffusion terms cancel. Therefore, the diffusion coefficient is a free parameter in the NDA calculation. We chose to use a nonlocal definition of a diffusion coefficient. The derivation was first proposed by Morel [10, 11] and later studied by Larsen and Trahan [5, 6]. This approach gives us a diffusion tensor $\underline{\underline{\mathrm{D}}}$ with

$$D_{ij} \equiv \int_{4\pi}(\boldsymbol{\Omega}\cdot\boldsymbol{e}_i)\left(\boldsymbol{\Omega}\cdot\boldsymbol{e}_j\right)f(\boldsymbol{\Omega})\,d\boldsymbol{\Omega} \quad (30)$$

where $f(\boldsymbol{\Omega})$ is the solution to

$$\boldsymbol{\Omega}\cdot\boldsymbol{\nabla}f+\sigma_{\mathrm{t}}f=\frac{1}{4\pi} \quad (31)$$
$$f(x_b,\boldsymbol{\Omega})=0. \qquad x_b\in\partial\mathcal{D},\boldsymbol{\Omega}\cdot\boldsymbol{n}<0. \quad (32)$$

This equation can be easily solved using any technique to solve a transport equation. In the case of an infinite homogeneous medium the nonlocal diffusion coefficient reduces to the classical local diffusion coefficient Eq. (22). In this study we obtain the nonlocal diffusion tensor from a WLS solve. Note that that the calculation does not require a scattering source, therefore no source iterations are necessary. The result is well defined in finite voids. Schunert at el. [12] showed that this diffusion coefficient can improve convergence properties of the NDA in problems with discontinuity of material properties.

In addition to the diffusion coefficient, the Eddington form of the current in the drift vector formulation Eq. (21) becomes singular in voids. We can also write the drift vector as

$$\hat{D}=-\boldsymbol{J}-\mathrm{D}\boldsymbol{\nabla}\phi. \quad (33)$$

The Eddington or pressure formulation for the current used in Eq. (21)

$$\boldsymbol{J}=-\frac{1}{\sigma_{\mathrm{tr}}}\sum_{m=1}^{M}\omega_m\boldsymbol{\Omega}_m(\boldsymbol{\Omega}_m\cdot\boldsymbol{\nabla}\psi_m) \quad (34)$$

can be replaced by the alternative of the direct or first moment representation

$$\boldsymbol{J}=\sum_{m=1}^{M}\omega_m\boldsymbol{\Omega}_m\cdot\psi_{m,g}. \quad (35)$$

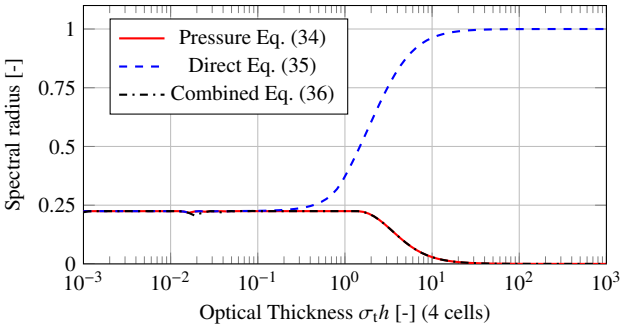

Fig. 1. Spectral radius for $c = 1$ as function of the cell thickness for the two formulations of the current and the combined formulation in a homogeneous material.

A Fourier analysis (Fig. 1) showed that the direct formulation shows convergence issues for optical thick cells. The reason for this is that the classical formulation results in a finite difference discretization scheme, skipping the center node. For high frequencies, this cannot resolve the first derivative correctly. However, voids are optically thin, therefore we choose to use

$$\boldsymbol{J}\equiv\begin{cases}-\frac{1}{\sigma_{\mathrm{tr}}}\sum_{m=1}^{M}\omega_m\boldsymbol{\Omega}(\boldsymbol{\Omega}_m\cdot\boldsymbol{\nabla}\psi_m) & ,\sigma_{\mathrm{tr}}h\geq\hat{\zeta}\\ \sum_{m=1}^{M}\omega_m\boldsymbol{\Omega}_m\cdot\psi_m & ,\sigma_{\mathrm{tr}}h<\hat{\zeta}\end{cases} \quad (36)$$

where $\hat{\zeta}$ is a threshold value for the optical thickness to switch between the two formulations and h is a characteristic length of the cell. Taking Fig. 1 into account $\hat{\zeta} = 0.01$ should provide good convergence for all optical thicknesses. It is verified numerically that this combined formulation Eq. (36) has the same convergence properties for a homogeneous material as the pressure formulation of the current.

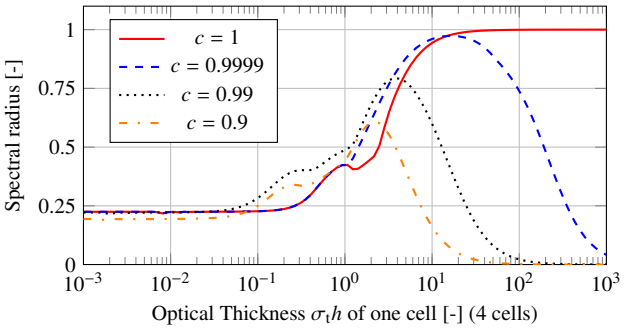

Fig. 2. Spectral radius for the combined drift vector formulation (Eq. (36)) as function of the cell thickness in a heterogeneous problem with a void and a material region with 2 cells each.

TABLE I. Maximal spectral radii for the combined drift vector formulation in a two material problem with a void

Scattering ratio c	Spectral radius ρ
1	1.0000
0.9999	0.9603
0.99	0.7936
0.9	0.6080

Figure 2 shows the result for a Fourier analysis using a two region periodic problem. The problem consists of a void and a highly diffusive material. It can be seen in the plot that the spectral radius for the scattering ratio $c = 1$ still goes to one, even though we use the combined formulation for the current (Eq. (36)) for the drift vector. However, for $c < 1$ we see, that the spectral radius does not approach one and the scheme converges unconditionally. Table I shows that for $c < 1$ the NDA void scheme accelerates the convergence.

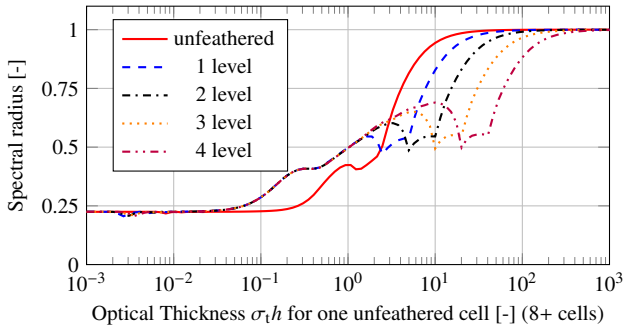

Fig. 3. Influence of different levels of feathering of the interface cell on the spectral radius for the combined drift vector formulation (Eq. (36)) with $c = 1$ in a heterogeneous problem with a void and a material region.

Figure 2 shows that for optical thick cells and high scattering ratios the acceleration scheme looses effectiveness. This is caused by an interface between an optically very thick cell and a very thin cell. To improve convergence we studied the effect of introducing cells of intermediate optical thickness. The last interface cells in the material are increasingly refined towards the void, creating a series of cells with decreasing optical thickness towards the void region. Every level of feathering means that the cells next to the void is divided by two, hence a level three feathering produces an interface with cells of $\frac{h}{2}$, $\frac{h}{4}$ and two with $\frac{h}{8}$ thickness. Figure 3 shows that this procedure moves the practical optical thickness, for which the scheme looses effectiveness to optically thicker cells. This, however, comes with the price of having more spatial cells in the problem. The implemented feathering scheme was only intended for a test and is by no means optimal.

4. SAAF Transport Equation with void treatment

The standard SAAF equation is not defined in voids. Wang et al.[13] proposed a modified version of the SAAF equation that is well defined in voids. Here we shall give a short derivation of the self-adjoint angular-flux equation with void treatment (SAAFτ). Further details are described in the paper by Wang.

Consider for the one group, isotropic case the first order transport equation. Solving for the angular flux gives

$$\psi = \frac{1}{\sigma_t}\left(-\boldsymbol{\Omega}\cdot\boldsymbol{\nabla}\psi + \frac{\sigma_s}{4\pi}\phi + \frac{q}{4\pi}\right). \tag{37}$$

We define the stabilization parameter τ as a function of a cell's optical thickness

$$\tau \equiv \begin{cases} \frac{1}{\sigma_t}, & \sigma_t h \geq \zeta \\ \frac{h}{\zeta}, & \sigma_t h < \zeta \end{cases} \tag{38}$$

with ζ the stabilization threshold, normally set to 0.5. First we subtract and add $\tau\sigma_{t,\psi}$ to ψ to obtain

$$\psi = (1-\tau\sigma_t)\,\psi + \tau\sigma_t\psi \tag{39a}$$

Next we substitute Eq. (37) into the last term of Eq. (39a) to get

$$\psi = (1-\tau\sigma_t)\,\psi + \tau\left(\frac{\sigma_s}{4\pi}\phi + \frac{q}{4\pi} - \boldsymbol{\Omega}\cdot\boldsymbol{\nabla}\psi\right) \tag{39b}$$

Substituting from Eq. (39b) into the streaming term of the transport equation Eq. (1) we get the SAAFτ equation

$$\begin{aligned} -\boldsymbol{\Omega}\cdot\boldsymbol{\nabla}\left[\tau\boldsymbol{\Omega}\cdot\boldsymbol{\nabla}\psi\right] + \boldsymbol{\Omega}\cdot\boldsymbol{\nabla}\left[(1-\sigma_t\tau)\,\psi\right] + \sigma_t\psi \\ = -\boldsymbol{\Omega}\cdot\boldsymbol{\nabla}\left[\tau\left(\frac{\sigma_s}{4\pi}\phi + \frac{q}{4\pi}\right)\right] + \frac{\sigma_s}{4\pi}\phi + \frac{q}{4\pi} \end{aligned} \tag{40}$$

This equation are compatible with voids, however the system matrix is not symmetric anymore due to the first derivative.

The NDA for the SAAFτ equation is consistent. It is derived from the P_0 projection of Eq. (40). The resulting low order equation is equal to Eq. (23) and the boundary condition is Eq. (26). The drift for the correction is

$$\begin{aligned} \hat{D} \equiv \frac{1}{\phi^{k+\frac{1}{2}}}\Bigg(\tau\sum_{m=1}^{M}\boldsymbol{\Omega}_m\cdot\boldsymbol{\Omega}_m\cdot\boldsymbol{\nabla}\psi_m \\ -\left[(1-\tau\sigma_t)\boldsymbol{J}\right] - \mathrm{D}\boldsymbol{\nabla}\phi\Bigg) \end{aligned} \tag{41}$$

For a given iteration k the SAAFτ NDA scheme is defined as follows:

1. Solve the SAAFτ transport equation

$$\begin{aligned} &\left(\tau\boldsymbol{\Omega}\cdot\boldsymbol{\nabla}\psi_m^{k+\frac{1}{2}}, \boldsymbol{\Omega}\cdot\boldsymbol{\nabla}\psi^*\right)_{\mathcal{D}} + \left((1-\sigma_t\tau)\,\psi_m^{k+\frac{1}{2}}, \boldsymbol{\Omega}\cdot\boldsymbol{\nabla}\right)_{\mathcal{D}} \\ &\quad + \left(\sigma_t\psi_m^{k+\frac{1}{2}}, \psi^*\right)_{\mathcal{D}} + \left\langle\psi_m^{k+\frac{1}{2}}, (\boldsymbol{\Omega}\cdot\boldsymbol{n})\,\psi^*\right\rangle_{\partial\mathcal{D}} \\ &= \left(\sum_{l=0}^{L}\sum_{p=-l}^{l}\frac{2l+1}{4\pi}\mathrm{Y}_l^p\sigma_{sl}\phi_l^{p,k}, \tau\boldsymbol{\Omega}\cdot\boldsymbol{\nabla}\psi^* + \psi^*\right)_{\mathcal{D}} \\ &\quad + \left(\frac{1}{4\pi}\bar{\nu}\sigma_f\phi^k + \frac{q}{4\pi}, \tau\boldsymbol{\Omega}\cdot\boldsymbol{\nabla}\psi^* + \psi^*\right)_{\mathcal{D}}, m = 1\ldots M \end{aligned} \tag{42a}$$

2. Calculate the correction terms for the diffusion equation

$$\kappa^{k+\frac{1}{2}} = \frac{4}{\phi} \sum_{\boldsymbol{n}\cdot\boldsymbol{\Omega}_m>0} \omega_m \left|\boldsymbol{n}\cdot\boldsymbol{\Omega}_m\right| \psi_m^{k+\frac{1}{2}} \tag{42b}$$

$$\hat{D}^{k+\frac{1}{2}} \equiv \frac{1}{\phi^{k+\frac{1}{2}}} \left(\tau \sum_{m=1}^{M} \boldsymbol{\Omega}_m \cdot \boldsymbol{\Omega}_m \cdot \boldsymbol{\nabla} \psi_m^{k+\frac{1}{2}} - \left[(1-\tau\sigma_t)\boldsymbol{J}^{k+\frac{1}{2}} \right] - \mathrm{D}\boldsymbol{\nabla}\phi^{k+\frac{1}{2}} \right) \tag{42c}$$

3. Solve the diffusion equation

$$-\left(\mathrm{D}\boldsymbol{\nabla}\phi^{k+1}, \boldsymbol{\nabla}\phi^*\right)_{\mathcal{D}} - \left(\hat{D}^{k+\frac{1}{2}}\phi^{k+1}, \boldsymbol{\nabla}\phi^*\right)_{\mathcal{D}} + \left\langle \frac{\kappa^{k+\frac{1}{2}}}{4}\phi^{k+1} - J^{\mathrm{in}}, \phi^* \right\rangle_{\partial\mathcal{D}} + \left(\sigma_a\phi^{k+1}, \phi^*\right)_{\mathcal{D}} = (q, \phi^*)_{\mathcal{D}} \tag{42d}$$

4. Check convergence and update the scattering source

With the nonlocal diffusion coefficient Eq. (30) this NDA scheme is also well defined in voids. We will use this NDA scheme to compare to our newly developed WLS NDA algorithm Eq. (28).

III. RESULTS AND ANALYSIS

1. Material Interface with Weighted Least-Squares

To test the WLS equation, consider a one dimensional problem with two material regions. The left region contains a weak absorber ($\sigma_t = 0.1\,\frac{1}{\mathrm{cm}}$), while the right region has a strong absorber ($\sigma_t = 10\,\frac{1}{\mathrm{cm}}$). Each region is 1 cm thick and the problem is surrounded by vacuum. A constant source of $q = 1\,\frac{\mathrm{n}}{\mathrm{s}}$ is added in both regions. We compare the unweighted LS to the weighted LS and the SAAF implementation with void treatment (SAAFτ) [13] in Rattlesnake. LS and WLS formulations use the boundary condition Eq. (12) and all calculations employ a S_8 Gauss quadrature.

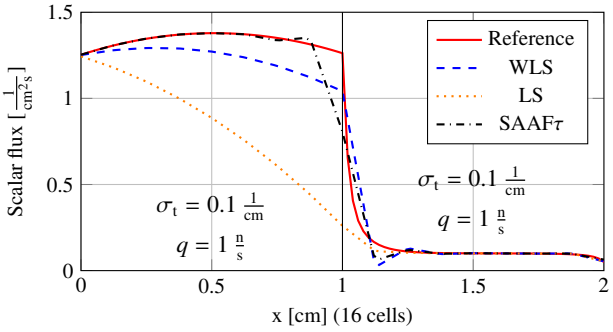

Fig. 4. Comparison of the scalar flux results for the two absorber problem

Figure 4 shows the results for the scalar flux. The LS result in the left half of the problem is strongly influenced by the thick material in the right half. The introduction of the weight function for the WLS ameliorates this problem, however the result shows still a decrease of the scalar flux towards the thick material. The SAAFτ scheme is closest to the reference solution, however it has a strong decrease in the cell next to the material interface.

The angular fluxes show that the error for the WLS scheme is strongly dependent on the angle. Only directions going from the thin into the thick half have the decrease in flux strength. The opposite direction is not influenced by the thin material region before the interface. The more perpendicular the positive direction to the interface is, the larger the error.

2. Reed's Problem

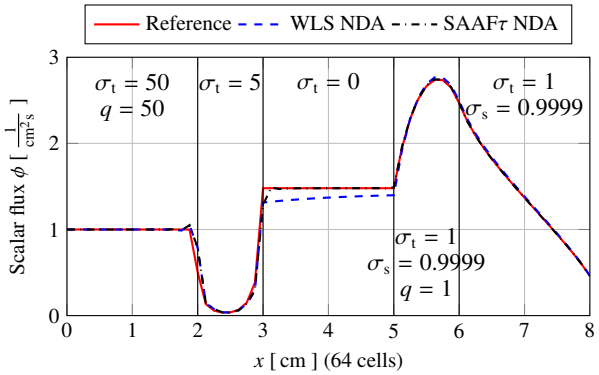

Fig. 5. Solution for the modified Reed's problem with SAAF NDA and LS NDA and comparison to a highly refined WLS reference solution. (Cross sections in $\frac{1}{\mathrm{cm}}$ and source strengths in $\frac{\mathrm{n}}{\mathrm{s}}$)

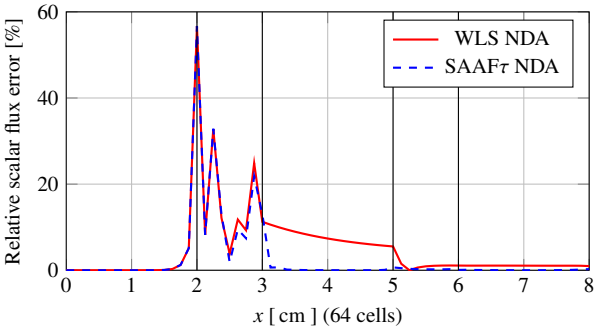

Fig. 6. Relative error for the modified Reed's problem with SAAF NDA and LS NDA to the WLS reference solution.

To test the void NDA modifications, we use a slightly modified version of Reed's problem, a well know test problem containing a void region and a highly diffusive region. The calculations uses both NDA schemes, the WLS Eq. (28) and the SAAFτ Eq. (42). The results are shown in Fig. 5 and the relative error in the scalar flux can be seen in Fig. 6. Both schemes have large errors in the absorber region. In the void region the WLS solution shows a non constant flux and a wrong magnitude. This affects the adjacent scattering region. The SAAFτ solution shows some small oscillations at the void's left boundary and a decrease in the scalar flux only in

the leftmost cell in the void. These inaccuracies in both WLS and SAAFτ disappear with increasing mesh refinement.

Both schemes needed 16 iterations to reduce the error between two consecutive low order solutions below the error tolerance of 10^{-10}. The SAAFτ scheme is consistent, hence the difference between high-order and low order solution can also be used as measurement for the error. It took only 14 iterations to reduce the iterative error below the tolerance. The WLS scheme is inconsistent and therefore the high-order and low-order solutions only converge in the limit of spatial refinement.

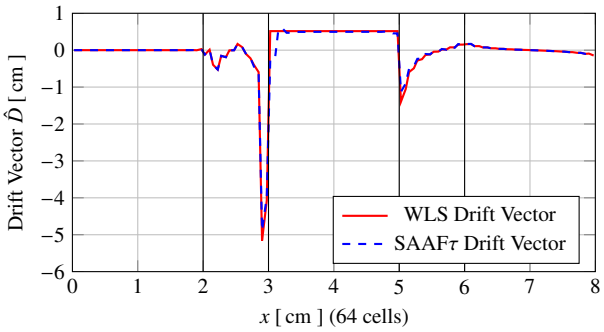

Fig. 7. Drift vectors for the LS and SAAF NDA calculation for Reed's problem

The drift vectors from both WLS and SAAFτ agree well as can be seen in Fig. 7. The SAAFτ drift vector has oscillation on the left side of the void region. The WLS drift vector is constant throughout the void region.

3. Two region problem with a void

To further investigate the non-constant flux of the WLS solution in the void region as shown in Fig. 5 we simplified the problem to an one dimensional two absorber problem. The left half of the problem contains a void ($\sigma_t = 0\ \frac{1}{cm}$), while the right side contains a strong absorber ($\sigma_t = 10\ \frac{1}{cm}$). On the left boundary is an incident isotropic flux $\phi_{in} = 1.0\ \frac{1}{cm^2 s}$.

In the void region the drift vector $\hat{D}_1 = -0.5$ is constant as well as the nonlocal diffusion coefficient D_1. Equation (23) simplifies in the void region to

$$-D_1 \frac{\partial^2}{\partial x^2}\phi_1 - \hat{D}_1 \frac{\partial}{\partial x}\phi_1 = 0 \tag{43}$$

where the subscript 1 stands for the left half of the problem. The analytical solution to Eq. (43) is

$$\phi_1(x) = A_1 + B_1 e^{-\frac{\hat{D}_1}{D_1}x} \tag{44}$$

with A_1 and B_1 constants to be determined by the boundary and interface conditions. As we can see, the constant solution is part of the solution space of Eq. (44) but not the only one. For a nonzero constant B_1 the solution can also be exponential.

The solution Eq. (44) in the void region is conservative. This can be easily shown using the current Eq. (20) with the solution Eq. (44) and substitute this into the balance equation Eq. (16).

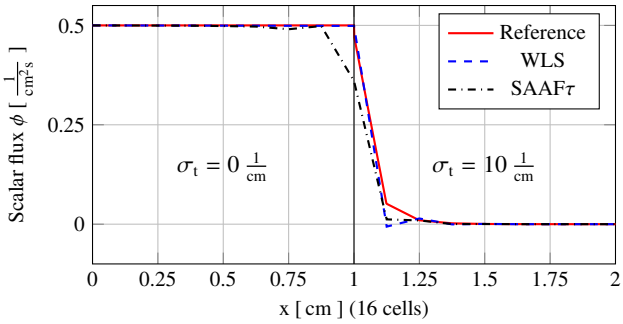

Fig. 8. Transport solutions for the two absorber problem with a void and an incident isotropic flux on the left side

Figure 8 shows the solution to the problem using the WLS and SAAFτ transport solvers. The WLS scheme shows an almost constant flux in the void region. The SAAFτ scheme starts oscillating towards the right side of the void region and drops in the last cell before the material interface. Both schemes have a dip after the interface in the material half and continuing oscillations into the material region.

The posed problem can be easily solved analytical and all correction terms can be derived from that analytical solutions. No scattering is present in the problem therefore no iterative solution is necessary. The low order solution can be obtained by feeding in a drift vector and vacuum boundary coefficient into a drift-diffusion solver. This allows the comparison of the analytical and numerical drift vectors and their influence on the NDA solution. The analytic case uses the drift vector obtained from the analytical angular flux and and integrated with S_8 quadrature. The numerical drift vectors were obtained from the transport solutions shown in Fig. 8 and use their corresponding formulation for the drift vector (WLS Eq. (28c) and SAAFτ Eq. (42c)).

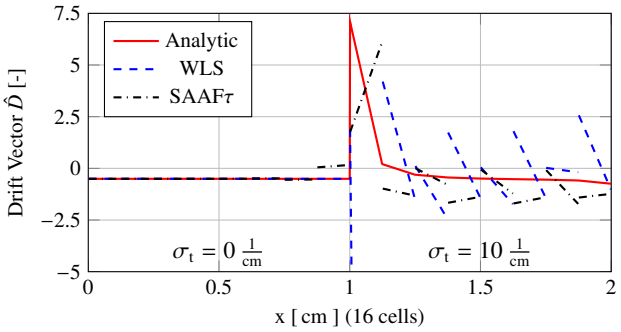

Fig. 9. Analytic and numerical drift vectors for the two absorber problem

Figure 9 shows the drift vectors. All drift vectors are negative and constant in the void, however the SAAFτ one starts oscillating towards the material interface and is positive in the last void cell before the interface. In the material region the drift vector results are far off the reference of the analytic drift vector. The reasons are that the transport solutions oscillate and that the low magnitude of the scalar flux ϕ makes the drift vector ill-conditions (Eqs. (21) and (41)). The numerical drift vectors are discontinuous.

Figure 10 shows the NDA solutions with the drift vectors

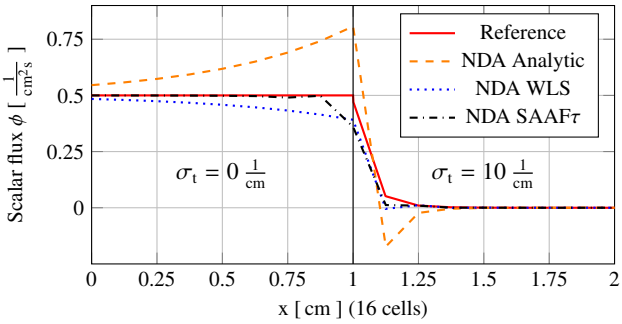

Fig. 10. NDA solutions to the two absorber problem with a void and an incident isotropic flux on the left side using different NDA schemes.

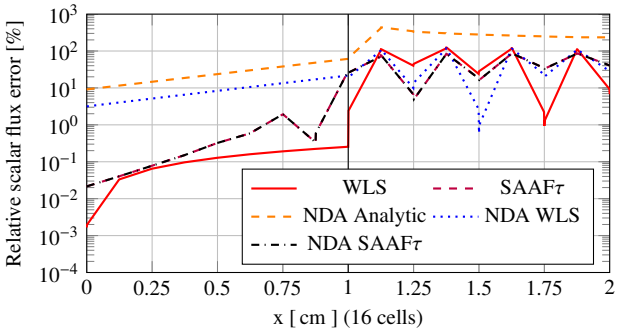

Fig. 11. Relative error in the scalar flux of the transport and NDA solutions for the two absorber problem with a void, the NDA solutions use different drift vector vectors.

described above. All calculation use an analytic expression for the nonlocal diffusion coefficient. Surprisingly the analytic drift vector gives the worst result. The scalar flux in the void region is exponentially increasing towards the material interface. The WLS drift vector produces a decreasing flux in the void regions. The SAAFτ is constant in the void region with minor oscillations except for the last cell before the interface. In this cell it decreases strongly. The results show that a more accurate drift vector does not necessarily increase the accuracy of the NDA solution.

The relative error in the scalar flux is shown in Fig. 11. The largest error shows the NDA with the analytic drift vector. In the void region the WLS transport solution has the least error. The SAAFτ transport and the NDA using the SAAFτ drift vector have almost exactly the same error. All numerical schemes show approximately the same error in the material region with strong oscillations.

To measure the influence of the drift vector formulation (Eq. (21) or Eq. (41)), the formulations are used with the other transport scheme, hence Eq. (42c) uses the transport solution from Eq. (28a) (labeled with NDA 1) and respectively Eq. (28c) the solution from Eq. (42a) (labeled with NDA 2). Figure 12 shows the comparison of the switched drift vectors with the original schemes and the corresponding relative errors are shown in Fig. 13. The drift vector formulation switch influences the solution only in the void part of the problem. For SAAFτ NDA the consistent schemes shows significant lower error than the NDA 2 scheme using the same transport

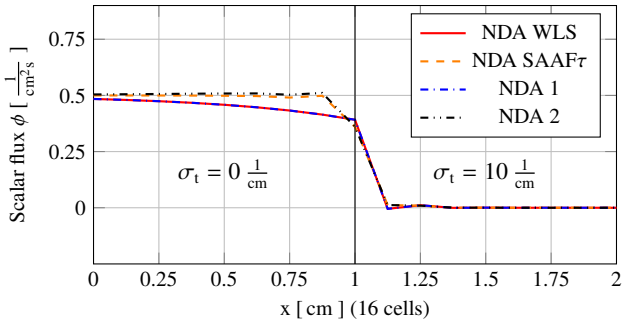

Fig. 12. Comparison of the NDA solutions to the two absorber problem with switched drift vectors.

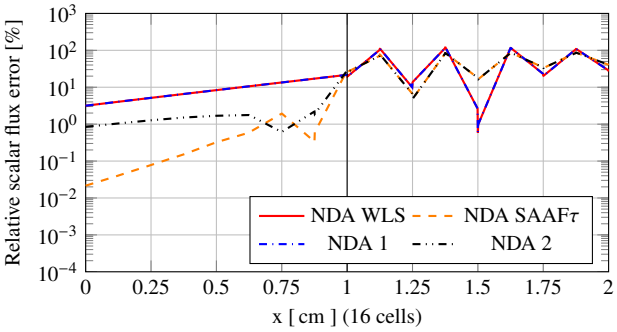

Fig. 13. Relative error in the scalar flux of the NDA solutions for the two absorber problem with switched drift vectors.

solution. The WLS NDA scheme error is comparable to the NDA 1 scheme. This shows that the NDA results are mainly dependent on the transport solution, and that the formulation of the drift vector is not the cause of the large deviations for the WLS scheme. This is particular interesting, since the WLS transport solution shows a smaller error in the void than the SAAFτ one (Fig. 11).

The described error in the void is a coarse mesh problem. Increasing refinement of the mesh reduces the error as shown in Fig. 14. All schemes converge spatially with second order. So do the schemes using the switched formulation of the drift vector (not shown to keep the plot simple). The convergence for NDA 1 is similar to the NDA WLS scheme and the convergence of NDA 2 is similar to the NDA SAAFτ.

IV. CONCLUSIONS

We derived a weighted LS transport equations and showed that we can make this equation equivalent to the SAAF equation by deploying the right weight function. However, to be able to handle voids, a modified weight function and optional boundary conditions are used, which renders the equations equal only for sufficient large cross sections and on the mesh interior. Even if the weight function does not completely guarantee causality for the WLS equation, the results improved significantly. The resulting discretization of the WLS scheme is in problems with void, in contrast to the SAAFτ scheme, symmetric positive definite.

The NDA was modified to support void regions by using a nonlocal diffusion tensor and an alternative formulation for

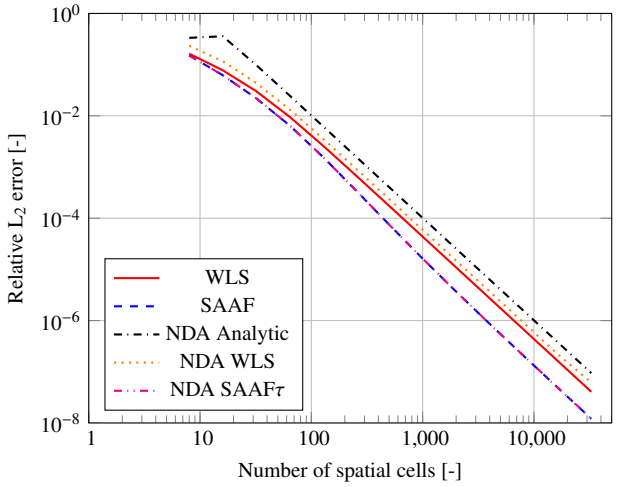

Fig. 14. Convergence of the error for the two region problem for transport and NDA solutions

the current in optical thin cells. The resultant algorithm loses effectiveness for problems with optical thick purely scattering cells and voids. However, for scattering ratios smaller than one the scheme accelerates the convergence. Materials in practical problems are never purely scattering.

The NDA results for the WLS show non-constant behavior in void regions. We showed that this solution is conservative and within the solution space of the drift-diffusion equation. Improved accuracy of the drift vector does not ameliorate the error in the void region. Currently different ways of improving the behavior of the NDA in the void region are under investigation.

ACKNOWLEDGMENTS

This material is based upon work supported by the Department of Energy, Battelle Energy Alliance, LLC, under Award Number DE-AC07-05ID14517.

REFERENCES

1. D. GASTON, C. NEWMAN, G. HANSEN, and D. LEBRUN-GRANDIE, "MOOSE: A Parallel Computational Framework for Coupled Systems of Nonlinear Equations," *Nuclear Engineering and Design*, **239**, *10*, 1768–1778 (2009).
2. J. HANSEN, J. R. PETERSON, J. E. MOREL, J. C. RAGUSA, and Y. WANG, "A Least-Squares Transport Equation Compatible with Voids," *Journal of Computational and Theoretical Transport*, **43**, *1-7*, 374–401 (2014).
3. J. MOREL and J. MCGHEE, "A Self-Adjoint Angular Flux Equation," *Nuclear Science and Engineering*, **132**, *3*, 312–25 (Jul. 1999).
4. J. R. PETERSON, H. R. HAMMER, J. E. MOREL, J. C. RAGUSA, and Y. WANG, "Conservative Nonlinear Diffusion Acceleration Applied to the Unweighted Least-Squares Transport Equation in MOOSE," in "Mathematics and Computations, Supercomputing in Nuclear Applications and Monte Carlo International Conference, M and C+SNA+MC 2015, April 19, 2015 - April 23, 2015," American Nuclear Society (2015), vol. 1, pp. 636–648.
5. E. W. LARSEN and T. J. TRAHAN, "2-D Anisotropic Diffusion in Optically Thin Channels," in "2009 ANS Annual Meeting and Embedded Topical Meetings: Risk Management and 2009 Young Professionals Congress, November 15, 2009 - November 19, 2009," American Nuclear Society (2009), *Transactions of the American Nuclear Society*, vol. 101, pp. 387–389.
6. T. J. TRAHAN and E. W. LARSEN, "3-D Anisotropic Neutron Diffusion in Optically Thick Media with Optically Thin Channels," in "Proc. Intl. Conf. on Math. and Comput. Methods Applied to Nucl. Sci. Eng.(M&C 2011), Rio de Janeiro, Brazil, May 8," (2011), vol. 12.
7. C. DRUMM, W. FAN, A. BIELEN, and J. CHENHALL, "Least-Squares Finite-Element Algorithms in the SCEPTRE Radiation Transport Code," *Ann Arbor*, **1001**, 48109–2104 (2011).
8. V. M. LABOURE, Y. WANG, and M. D. DEHART, "Least-Squares PN Formulation of the Transport Equation Using Self-Adjoint-Angular-Flux Consistent Boundary Conditions," in "Physics of Reactors 2016: Unifying Theory and Experiments in the 21st Century, PHYSOR 2016, May 1, 2016 - May 5, 2016," American Nuclear Society (2016), *Physics of Reactors 2016, PHYSOR 2016: Unifying Theory and Experiments in the 21st Century*, vol. 5, pp. 3376–3385.
9. T. MANTEUFFEL and K. RESSEL, "Least-Squares Finite-Element Solution of the Neutron Transport Equation in Diffusive Regimes," *SIAM Journal on Numerical Analysis*, **35**, *2*, 806–35 (Apr. 1998).
10. J. E. MOREL, "A Non-Local Diffusion Theroy," Research Report LA-UR-07-5257, Los Alamos National Laboratory, NM (2007).
11. J. E. MOREL, J. S. WARSA, and K. G. BUDGE, "Alternative Generation of Non-Local Diffusion Tensors," Research memo, Texas A&M University (2010).
12. S. SCHUNERT, H. R. HAMMER, J. LOU, Y. WANG, J. ORTENSI, F. N. GLEICHER, B. BAKER, M. D. DEHART, and R. C. MARTINEAU, "Using Directional Diffusion Coefficients for Nonlinear Diffusion Acceleration of the First Order S N Equations in Near-Void Regions," Las Vegas, NV (Nov. 2016).
13. Y. WANG, H. ZHANG, and R. C. MARTINEAU, "Diffusion Acceleration Schemes for Self-Adjoint Angular Flux Formulation with a Void Treatment," *Nuclear Science and Engineering*, **176**, *2*, 201–225 (2014).